Hierarchical 3D Nanolayered Duplex-Phase Zr with High Strength, Strain Hardening, and Ductility

Jie-Wen Zhang, Irene J. Beyerlein, and Wei-Zhong Han

Phys. Rev. Lett. **122**, 255501 — Published 24 June 2019

DOI: 10.1103/PhysRevLett.122.255501

Hierarchical 3D Nanolayered Duplex-Phase Zr with High Strength, Strain Hardening, and Ductility

Jie-Wen Zhang[1], Irene J. Beyerlein[2*], Wei-Zhong Han[1*]

[1]Center for Advancing Materials Performance from the Nanoscale, State Key Laboratory for Mechanical Behavior of Materials, Xi'an Jiaotong University, Xi'an 710049, P.R. China

[2]Mechanical Engineering Department, Materials Department, University of California, Santa Barbara, CA 93106-5070, USA

Abstract: Nanolayered, bimetallic composites are receiving increased attention due to an exceptional combination of strength and thermal stability not possible from their coarse-layered counterparts or constituents alone. Yet, due to their 2D planar, unidirectional arrangement, they are highly anisotropic, which results in limited strain hardening and ductility. Therefore, like many high-performance, ultra-strong materials of our time, they succumb to the usual strength-ductility trade-offs. Here we present the formation of a novel hierarchical microstructure, comprised of crystals consisting of 3D nanolayered α/β-Zr networks. By direct comparison with coarse-layered material of the same chemistry, we show that the unusual hierarchical 3D structure gives rise to high strain hardening, high strength and high ductility. Using TEM analysis and hysteresis testing, we discovered that the 3D randomly oriented bi-phase boundaries result in progressively dispersive rather than localized slip with increasing strain. Dislocation activity in the α-Zr lamellae transitions from single slip to multi-slip and eventually to multi-modal slip as strain increases. The diffusive slip promoting properties of 3D layered networks can potentially invoke simultaneous high strength, strain hardening, and ductility, reveals a new target in the microstructural design of high performance structural materials.

Keywords: Hierarchical, Interfaces, Dislocation, Strength, Ductility

Zirconium (Zr) alloys are attracting considerable interest due to their excellent physical and chemical properties, such as small thermal neutron capture cross-section, corrosion resistance, etc. [1-7]. As a result, Zr alloys are extensively used in the nuclear industry as the pressure tubes and fuel claddings [8-11]. Because of ever-increasing demands on structural materials for new generation nuclear reactors, vast improvements in strength and ductility are critically needed. Most attempts to date involve alloying elements or tuning the internal microstructure [10-17]. While many of these methods enable high strength (>500 MPa), the ductility is still too low (<10%) [1,18], which limits tube fabrication and service life.

In addition to the strength-ductility trade-off, Zr alloys also exhibit severe irradiation-induced anisotropic growth [8]. In nuclear reactors, Zr alloy cladding tubes tend to grow in the axial direction and contract in the radial direction [8]. This radiation growth is a form of plasticity; it results from the accumulation and partitioning of point defects at preferred crystallographic planes [8]. Because of its sensitivity to crystallography, this directional growth is further exacerbated by a preferred texture.

It has long been envisioned that problems in-reactor growth and strengthening can be solved via the infusion of interfaces. Metallic multilayers have demonstrated 5 to 10 times higher strength than the coarser laminates, as well as enhanced thermal stability and radiation tolerance [19-28]. They owe these properties to a high density of bi-phase interfaces, which provide for strength and deformability by obstructing the motion of, annihilating, or storing dislocations [20-26], and radiation tolerance by acting as efficient sinks for defects [27-29]. High thermal stability emerges since the bi-phase interface has low interface energy [30,31].

In hopes of exploiting this nanostructure concept, several studies have considered interface-dominant Zr. For instance, two-phase Zr/Nb nanolayered composites have been made via magnetron sputtering [32-35] and accumulative roll bonding [36]. However, all the above techniques produce nearly 2D architecture of planar, stacked Zr/Nb layers, which renders their deformation response highly anisotropic. Further, these synthesis methods have their limitations in large-scale production [36-38]. Last, due to potential contamination in fabrication, these nanolaminated composites have weak interface bonding, which leads to poor ductility [39].

Here we present an unusual, two-phase Zr-2.5Nb nanostructured composites with a 3D network of nanolayers. The hierarchical 3D nanolayered sample consists of nearly equiaxed coarse grains filled with micro-scale colonies, each of which are nanolaminated with numerous

body-centered cubic (bcc)/hexagonal close-packed (hcp) interfaces. The 3D layered networks give rise to high yield strength, strain hardening and ductility, making it a promising hierarchical microstructure for harsh conditions.

Figure 1(a) shows a typical Zr-Nb binary phase diagram. The red-dashed line marks the composition of the alloy. The eutectoid decomposition is sluggish at a temperature below 610℃ [40,41]. Consequently, the microstructure at room temperature is expected to consist of α-Zr with < 0.6wt.% Nb and a metastable β-Zr with < 20wt.% Nb. On this basis, a traditional method was used to prepare a coarse-layered (CL) Zr-2.5Nb alloy (see supplementary materials (SM)). A layered structure with alternating α- and β-Zr phases has formed, as shown in Fig. 1(b). The darker one is the α-Zr phase and the brighter one is the β-Zr phase. Fig. 1(c) presents a statistical analysis of layer thickness of the α phase. Most of the α phase lamellae (>90%) have a thickness smaller than 1 μm, with an average value of 589±227 nm. Although this sample has a layered microstructure, the interface density (3.25 μm^{-1}, number of interfaces per unit length) is not exceptionally high, and the thickness distribution of the α phase is heterogeneous (Fig. 1(c)).

To create a more refined, two-phase nanostructure, we designed the dynamic thermal-mechanical phase transformation (DTMPT), as shown in Fig. 1(d) and SM. Fig. 1(d) displays an image of the "bulk" disc sample with a diameter of 35 mm and thickness of 7 mm. In the micron-scale colonies, the α/β-Zr layers and interfaces are distributed homogeneously (Fig. 1(e)). The interface planes randomly oriented in the same colony and not stacked, in a planar arrangement as in the CL Zr-2.5Nb [32-36]. The α layers are shorter and thinner as well. Most of the α phases start and terminate in the center of grain, indicating that the precipitation of the α phase not only originated from the grain boundaries but also from locations within the interior of the grains [42,43]. The α/β lamellar structure are on average 222±94 nm (Fig. 1(c)). The thickness of the majority (>90%) of α phase is less than 350 nm. The DTMPT sample has a much higher interface density (8.25 μm^{-1}) than the CL sample.

Fig. 2 shows a typical TEM image of the α/β-Zr phase nanostructure in an individual colony. The α layer and nano-scale β layer with thickness of 10 to 20 nm are stacked within a single colony. According to the diffraction pattern in Fig. 2(b), the interface has a classical Burgers orientation relationship $[0001]_\alpha // [011]_\beta$ and $(\bar{1}\bar{1}20)_\alpha // (1\bar{1}1)_\beta$ between the α and β phases. Because the hierarchical 3D structure is formed by a phase transformation from the β to α phase,

the orientation of the β phase is similar within one grain. However, the α phases in the various colonies are of different variants although they were inherited from the same β grain. Therefore, the bonding between the two phases is clean and contamination-free. The α/β interface is not atomically flat (Fig. 2(c)), but is comprised of a series of facets, which can facilitate dislocation nucleation at the α/β interface [44]. Meanwhile, the misfit strain along the $[\bar{1}\bar{1}20]_\alpha$ and $[0001]_\alpha$ is 5.0% and 2.6%, indicating that the α/β interface is semi-coherent and has interface dislocations. The interface plane is near $(\bar{1}100)$ for α phase and $(\bar{2}\bar{1}1)$ plane for β phase (Fig. 2(b)). The $(10\bar{1}0)$ prismatic plane in the hcp α phase is almost parallel to the $(0\bar{1}1)$ plane in bcc β phase. The well-aligned planes across the interface can provide a favorable pathway for slip to transfer across it [45].

The hierarchical 3D nanolayered and CL Zr-2.5Nb are tested in tension to evaluate their mechanical response. The hierarchical 3D sample exhibits the higher yield strength ($\sigma_{0.2} \approx 576$ MPa) and higher ultimate tensile strength ($\sigma_b \approx 693$ MPa) compared to the CL sample with $\sigma_{0.2} \approx 511$ MPa and $\sigma_b \approx 621$ MPa, as shown in Fig. 3(a). The total elongation of hierarchical 3D Zr-2.5Nb ($\delta \approx 16.6\%$) is larger than that of CL sample ($\delta \approx 13.3\%$). The high strain hardening rate of the hierarchical 3D sample is also much higher (Fig. S1). Simultaneous yield and ultimate tensile strengths, ductility, and strain hardening is unusual for a nanostructured metal [46].

Figure 4 plots the strength versus uniform elongation of hierarchical 3D layered Zr-2.5Nb and other Zr alloys [47-53]. In this plot, two distinct groups emerge. The coarser-grained or ultra-fined grained Zr lie in group I, where the strength-ductility trade-off is strong. The second group consists of both nanostructured and heterogeneous microstructured Zr alloys. The group II is superior to group I since the strengths and ductility are higher; nonetheless, the trade-off exists. The hierarchical 3D layered Zr-2.5Nb lies in the center of group II, which means it achieves a balance of both strength and uniform elongation. The high strain hardening rate and uniform tensile ductility are attributed to the steep strain gradients resulting from the semi-coherent interfaces [54,55], and locally non-uniform plastic deformation across the microstructure. In contrast, the CL Zr-2.5Nb belongs to the group I of Zr alloys with inferior mechanical properties (Fig. 4). Comparatively other Zr alloys in group II have lower ductility and lower strain hardening. Generally, these reductions have been attributed to insufficient space for dislocation accumulation within crystals of nanoscale dimensions [24-26]. In spite of being

nanostructured as well, the hierarchical 3D Zr alloy evidently exhibits better mechanical performance. This could imply that the α/β interfaces are acting not only as strong barriers to dislocation motion but also assist dislocations accumulating in the layers.

To quantify the dislocation accumulation induced strain hardening, we measure the magnitude of the back stress during tensile in Fig. 3(b). The back stress is the long-range stress generated by dislocations that pile up against microstructural barriers, such as the α/β interfaces. This stress has polarity; it acts "back" on the dislocation sources, which lie within the α/β interfaces as well. For both the hierarchical 3D and CL samples, the hysteresis loops increase in size as the strain level increases from 2.5% to 3.0% (Fig. S1). The size of the loop is larger for the hierarchical 3D sample than the CL sample. The back stress of both hierarchical 3D and CL Zr-2.5Nb increases linearly with strain (Fig. 3(b)). Notably the hierarchical 3D sample has a larger slope and a higher value, which explains the stronger strain hardening rate.

The hysteresis analysis indicates considerable and continual accumulation of dislocations at the α/β interfaces. Using TEM, we attempt to identify the character of dislocations accumulated at different stages in the tensile response, as marked in Fig. 5(a). The first tensile test is interrupted at $\sigma_e \approx 230$ MPa. Although the whole sample is deforming elastically, we find substantial dislocation activity in the α-Zr layers. Fig. 5(b) shows typical dislocation structures form inside the α-Zr layers. Under the viewing direction of $[0001]_\alpha$, the α/β interface is near edge-on [56]. Several dislocation lines, corresponding to prismatic $\langle\vec{a}\rangle$ slip, are observed inside the α layers on the $(0\bar{1}10)$ prismatic plane, as marked in Fig. 5(b). One plane of glide is preferred, and the interface causes them to pile up (ρ=7 μm^{-1}, number of dislocation per unit length along interface).

To see if these same types of dislocations pile up as strain is increased, a second tensile test was interrupted at $\sigma_e \approx 394$ MPa, which lies in the middle of bulk elastic deformation but before macroscopic yielding. The dominant slip plane is still the same prismatic $(0\bar{1}10)$ plane, as shown in Figs. 5(c) and (d). However, numerous dislocation, with a density of ρ = 10.25 μm^{-1} pile-up along the α/β interface, as indicated by the strong strain contours formed at the interface. The increased number of pile-ups of dislocations along the α/β interfaces would generate an even larger back stresses. Again, the increase in back stress is an indication of high interface barrier strength and an effective strain hardening mechanism.

The third tensile test is interrupted at the macroscopic elastic-plastic transition, which is at $\sigma_e \approx 587$ MPa. At this point, dislocations are no longer gliding on a single preferred plane but on the three distinct prismatic planes, as marked in Fig. 5(e). The strain contours formed on the α/β interface, consequently, are more intense (ρ=16.8 μm^{-1}), indicating strong dislocation-interface interactions (Fig. 5(f)). Activation of non-planar systems promotes homogeneity in deformation, and postpones localization instabilities, while increasing dislocation accumulation, explaining the high hardening rate and improved ductility.

The final tensile test was stopped at the peak stress, $\sigma_e \approx 693$ MPa. A higher density of dislocations gliding on the three differently oriented prismatic planes is observed, as marked in Fig. 5(g). In addition, dislocation activity on the first-order <c+a> pyramidal plane $(10\bar{1}1)$ can be tracked (Fig. 5(h)). The dislocation should be out of contrast when its Burgers vector is parallel to the zone axis; therefore, the <c+a> dislocation observed here has a Burgers vector of $\frac{1}{3}[\bar{2}113]$. This is consistent with the principal dislocations located at the α/β interface [54,55]. These <c+a> interfacial dislocations may act as dislocation sources for the <c+a> dislocations observed in Fig. 5(h) and assist in accommodating plasticity along the crystal's c-axis. The spacing of these <c+a> misfit dislocations is about 10 nm [55], which is sufficiently dense to emit enough dislocations to mediate plasticity. Slip transmission events along $(0\bar{1}1)_\beta$-$(10\bar{1}0)_\alpha$ were identified at several locations, as highlighted in the upper left corner in Fig. 5(g). To this point, many dislocations gliding on different slip planes pile up along the α/β interfaces with ρ = 24.75 μm^{-1}. In addition, some dislocations are stored within the α layers, by the end of uniform deformation (Figs. 5(g) and (h)). With increasing storage of dislocations inside the α layers and slip transmission events, the rates of dynamic recovery of dislocations would be enhanced. The reduction in dislocation storage explains the reduced strain hardening rate and the transition from uniform deformation to localized deformation in the form of necking.

These TEM studies reveal that dislocation activity within the 3D networks becomes increasingly intricate, initializing as slip on a preferred system, then transitioning to multi-slip, and then eventually multi-modal slip as strain increases. Evidently, the 3D arrangement of nanolayers gives rise to an increasingly isotropic slip pattern, favorably leading to more homogeneous deformation, rather than an increasingly more localized form of slip. By dispersing slip with evolving with strain, the biphase interfaces have effectively not only strengthen the material but vastly improved its strain hardening and ductility. The generation of back stresses,

promoted by the α/β interfaces, led to the sequential activation of slip systems on differently oriented prismatic and pyramidal planes, which provided the large deformability of the hierarchical 3D nanolayered Zr-2.5Nb. The high density and 3D configuration of α/β interfaces plays a critical role in strengthening and strain hardening.

In summary, we present a bulk metal with a unique hierarchical 3D nanolayered microstructure, comprised of a high density of nano-scale duplex phases within micron-scale colonies, which are, in turn, located within grains tens of micrometers in diameter. The newly designed hierarchical 3D Zr alloy has a combination of high strength, strain hardening, and ductility. These novel mechanical properties can be attributed to the strengthening effect of the interfaces and activation of multiple slip systems. Because the DTMPT process can be easily advanced to industrial scales, it offers opportunties for designing high performance metals in sizes suitable for high performance structural applications.

*E-mails: wzhanxjtu@xjtu.edu.cn; beyerlein@ucsb.edu

Acknowledgements

This work was supported by the National Key Research and Development Program of China (2017YFB0702301), the National Natural Science Foundation of China (Grant Nos.51471128 and 51621063) and the 111 Project of China (Grant No. BP2018008). I.J.B was supported by the U.S. Department of Energy, Office of Science, Basic Energy Sciences (BES) under award DE-SC0018901. J.W.Z acknowledges Y.B.Q. for assistance.

References

[1] L. Balogh, D. W. Brown, P. Mosbrucker, F. Long, and M. R. Daymond, Dislocation structure evolution induced by irradiation and plastic deformation in the Zr-2.5Nb nuclear structural material determined by neutron diffraction line profile analysis, Acta Mater. **60,** 5567 (2012).

[2] R. V. Kulkarni, K. V. Mani Krishna, S. Neogy, D. Srivastava, E. Ramadasan, R. S. Shriwastaw, B. N. Rath, N. Saibaba, S. K. Jha, and G. K. Dey, Mechanical properties of Zr–2.5%Nb pressure tube material subjected to heat treatments in α + β phase field, J. Nucl. Mater. **451,** 300 (2014).

[3] D. G. Leo Prakash, M. Preuss, M. Dahlbäck, and J. Quinta da Fonseca, Microstructure and texture evolution during thermomechanical processing of β-quenched Zr, Acta Mater. **88,** 389 (2015).

[4] J. C. Gong, T. Benjamin Britton, M. A. Cuddihy, F. P. E. Dunne, and A. J. Wilkinson, <a> Prismatic, <a> basal, and <c+a> slip strengths of commercially pure Zr by micro-cantilever tests, Acta Mater. **96,** 249 (2015).
[5] M. Cottura, and E. Clouet, Solubility in Zr-Nb alloys from first-principles, Acta Mater. **144,** 21 (2018).
[6] M. Topping, T. Ungár, C. P. Race, A. Harte, A. Garner, F. Baxter, S. Dumbill, P. Frankel, and M. Preuss, Investigating the thermal stability of irradiation-induced damage in a zirconium alloy with novel in situ techniques, Acta Mater. **145,** 255 (2018).
[7] C. M. Silva, K. J. Leonard, E. V. Abel, J. Wilna Geringer, and C. D. Bryan, Investigation of mechanical and microstructural properties of Zircaloy-4 under different experimental conditions, J. Nucl. Mater. **499,** 546 (2018).
[8] R. A. Holt, In-reactor deformation of cold-worked Zr–2.5Nb pressure tubes, J. Nucl. Mater. **372,** 182 (2008).
[9] K. Holm, J. D. Embury, and G. R. Purdy, The structure and properties of microduplex Zr-Nb alloys, Acta Metall. **25,** 1191 (1977).
[10] R. Tewari, D. Srivastava, G. K. Dey, J. K. Chakravarty, and S. Banerjee, Microstructural evolution in zirconium based alloys, J. Nucl. Mater. **383,** 153 (2008).
[11] N. Saibaba, Kumar Vaibhaw, S. Neogy, K. V. Mani Krishna, S. K. Jha, C. Phani Babu, S. V. Ramana Rao, D. Srivastava, and G. K. Dey, Study of microstructure, texture and mechanical properties of Zr–2.5Nb alloy pressure tubes fabricated with different processing routes, J. Nucl. Mater. **440,** 319 (2013).
[12] M. Zhang, F. C. Zhang, Z. N. Yang, Y. N. Li, L. Qu, and H. J. Zhen, Effect of cooling process on the formation of duplex microstructure in Zr–2.3Nb alloy, J. Alloys Compd. **651,** 316 (2015).
[13] S. K. Jha, N. Keskar, K. I. Vishnu Narayan, K. V. Mani Krishna, D. Srivastava, G. K. Dey, and N. Saibaba, Microstructural and textural evolution during hot deformation of dilute Zr–Sn alloy, J. Nucl. Mater. **482,** 12 (2016).
[14] Q. S. Dong, H. B. Yu, Z. W. Yao, F. Long, L. Balogh, and M. R. Daymond, Study of microstructure and precipitates of a Zr–2.5Nb–0.5Cu CANDU spacer material, J. Nucl. Mater. **481,** 153 (2016).
[15] H. B. Yu, Z. W. Yao, and M. R. Daymond, The stability of thermodynamically metastable phases in a Zr–Sn–Nb–Mo alloy: Effects of alloying elements, morphology and applied stress/strain, J. Nucl. Mater. **493,** 84 (2017).
[16] Z. N. Yang, F. C. Zhang, F. C. Liu, Z. G. Yan, and Y. Y. Xiao, Achieving high strength and toughness in a Zr–2.3Nb alloy by the formation of duplex microstructure, Mater. Des. **40,** 400 (2012).
[17] M. Zhang, Y. N. Li, F. C. Zhang, X. B. Wang, L. Y. Chen, and Z. N. Yang, Effect of annealing treatment on the microstructure and mechanical properties of a duplex Zr–2.5Nb alloy, Mater. Sci. Eng. A **706,** 236 (2017).
[18] D. Fuloria, N. Kumar, S. Goel, R. Jayaganthan, S. Jha, and D. Srivastava, Tensile properties and microstructural evolution of Zircaloy–4 processed through rolling at different temperatures, Mater. Des. **103,** 40 (2016).
[19] W. Z. Han, M. J. Demkowicz, N. A. Mara, E. G. Fu, S. Sinha, A. D. Rollett, Y. Q. Wang, J. S. Carpenter, I. J. Beyerlein, and A. Misra, Design of radiation tolerant materials via interface engineering, Adv Mater. **25,** 6975 (2013).

[20] L. Lu, Y. F. Shen, X. H. Chen, L. H. Qian, and K. Lu, Ultrahigh strength and high electrical conductivity in copper, Science **304,** 422 (2004).
[21] A. Misra, J. P. Hirth, and R. G. Hoagland, Length-scale-dependent deformation mechanisms in incoherent metallic multilayered composites, Acta Mater. **53,** 4817 (2005).
[22] K. Lu, L. Lu, and S. Suresh, Strengthening materials by engineering coherent internal boundaries at the nanoscale, Science **324,** 349 (2009).
[23] I. J. Beyerlein, M. J. Demkowicz, A. Misra, and B. P. Uberuaga, Defect-interface interactions, Prog. Mater. Sci. **74,** 125 (2015).
[24] X. L. Wu, M. X. Yang, F. P. Yuan, G. L. Wu, Y. J. Wei, X. X. Huang, and Y. T. Zhu, Heterogeneous lamella structure unites ultrafine-grain strength with coarse-grain ductility, Proc. Natl. Acad. Sci. USA **112,** 14501 (2015).
[25] X. L. Wu, and Y. T. Zhu, Heterogeneous materials: a new class of materials with unprecedented mechanical properties, Mater. Res. Lett. **5,** 527 (2017).
[26] C. X. Huang, Y. F. Wang, X. L. Ma, S. Yin, H. W. Höppel, M. Göken, X. L. Wu, H. J. Gao, and Y. T. Zhu, Interface affected zone for optimal strength and ductility in heterogeneous laminate, Mater. Today. **21,** 713 (2018).
[27] G. Ackland, Controlling radiation damage, Science **327,** 1587 (2010).
[28] X. M. Bai, A. F. Voter, R. G. Hoagland, M. Nastasi, and B. P. Uberuaga, Efficient Annealing of Radiation Damage Near Grain Boundaries via Interstitial Emission, Science **327,** 1631 (2010).
[29] W. Z. Han, M. J. Demkowicz, E. G. Fu, Y. Q. Wang, and A. Misra, Effect of grain boundary character on sink efficiency, Acta Mater. **60,** 6341 (2012).
[30] A. Misra, and R. G. Hoagland, Effects of elevated temperature annealing on the structure and hardness of copper/niobium nanolayered films, J. Mater. Res. **20,** 2046 (2005).
[31] S. J. Zheng, I. J. Beyerlein, J. S. Carpenter, K. Kang, J. Wang, W. Z. Han, and N. A. Mara, High-strength and thermally stable bulk nanolayered composites due to twin-induced interfaces, Nat. Commun. **4,** 1696 (2013).
[32] M. Callisti, and T. Polcar, Combined size and texture-dependent deformation and strengthening mechanisms in Zr/Nb nano-multilayers, Acta Mater. **124,** 247 (2017).
[33] E. Frutos, M. Callisti, M. Karlik, and T. Polcar, Length-scale-dependent mechanical behavior of Zr/Nb multilayers as a function of individual layer thickness, Mater. Sci. Eng. A **632,** 137 (2015).
[34] M. Callisti, S. Lozano-Perez, and T. Polcar, Structural and mechanical properties of γ-irradiated Zr/Nb multilayer nanocomposites, Mater. Lett. **163,** 138 (2016).
[35] M. Callisti, M. Karlik, and T. Polcar, Competing mechanisms on the strength of ion-irradiated Zr/Nb nanoscale multilayers: Interface strength versus radiation hardening, Scripta Mater. **152,** 31 (2018).
[36] J. S. Carpenter, T. Nizolek, R. J. McCabe, M. Knezevic, S. J. Zheng, B. P. Eftink, J. E. Scott, S. C. Vogel, T. M. Pollock, N. A. Mara, and I. J. Beyerlein, Bulk texture evolution of nanolamellar Zr–Nb composites processed via accumulative roll bonding, Acta Mater. **92,** 97 (2015).
[37] M. Ardeljan, M. Knezevic, T. Nizolek, I. J. Beyerlein, N. A. Mara, and T. M. Pollock, A study of microstructure-driven strain localizations in two-phase polycrystalline HCP/BCC composites using a multi-scale model, Int. J. Plast. **74,** 35 (2015).

[38] M. Knezevic, T. Nizolek, M. Ardeljan, I. J. Beyerlein, N. A. Mara, and T. M. Pollock, Texture evolution in two-phase Zr/Nb lamellar composites during accumulative roll bonding, Int. J. Plast. **57,** 16 (2014).
[39] Y. Saito, H. Utsunomiya, N. Tsuji, and T. Sakai, Novel ultra-high straining process for bulk materials—development of the accumulative roll-bonding (ARB) process, Acta Mater. **47,** 579 (1999).
[40] S. Cai, M. R. Daymond, and R. A. Holt, Deformation of high β-phase fraction Zr–Nb alloys at room temperature, Acta Mater. **60,** 3355 (2012).
[41] M. Griffiths, J. E. Winegar, and A. Buyers, The transformation behaviour of the β-phase in Zr–2.5Nb pressure tubes, J. Nucl. Mater. **383,** 28 (2008).
[42] X. Li, F. Bottler, R. Spatschek, A. Schmitt, M. Heilmaier, and F. Stein, Coarsening kinetics of lamellar microstructures: Experiments and simulations on a fully-lamellar Fe-Al in situ composite, Acta Mater. **127,** 230 (2017).
[43] D. X. Wei, Y. Koizumi, M. Nagasako, and A. Chiba, Refinement of lamellar structures in Ti-Al alloy, Acta Mater. **125,** 81 (2017).
[44] R. F. Zhang, J. Wang, I. J. Beyerlein, A. Misra, T. C. Germann, Acta Mater. 60, 2885 (2012).
[45] Y. Matsukawa, I. Okuma, H. Muta, Y. Shinohara, R. Suzue, H. L. Yang, T. Maruyama, T. Toyama, J. J. Shen, Y. F. Li, Y. Satoh, S. Yamanaka, and H. Abe, Crystallographic analysis on atomic-plane parallelisms between bcc precipitates and hcp matrix in recrystallized Zr-2.5Nb alloys, Acta Mater. **126,** 86 (2017).
[46] I. A. Ovid'ko, R. Z. Valiev, and Y. T. Zhu, Review on superior strength and enhanced ductility of metallic nanomaterials, Prog. Mater. Sci. **94,** 462 (2018).
[47] L. Jiang, O. A. Ruano, M. E. Kassner, and M. T. Pérez-Prado, The Fabrication of Bulk Ultrafine-Grained Zirconium by Accumulative Roll Bonding, JOM **59**, 42 (2007).
[48] D. F. Guo, M. Li, Y. D. Shi, Z. B. Zhang, T. Y. Ma, H. T. Zhang, and X. Y. Zhang, Simultaneously enhancing the ductility and strength of cryorolled Zr via tailoring dislocation configurations, Mater. Sci. Eng. A **558**, 611 (2012).
[49] D. F. Guo, Z. B. Zhang, G. S. Zhang, M. Li, Y. D. Shi, T. Y. Ma, and X. Y. Zhang, An extraordinary enhancement of strain hardening in fine-grained zirconium, Mater. Sci. Eng. A **591**, 167 (2014).
[50] D. F. Guo, M. Li, Y. D. Shi, Z. B. Zhang, H. T. Zhang, X. M. Liu, B. N. Wei, and X. Y. Zhang, High strength and ductility in multimodal-structured Zr, Mater. Des. **34**, 275 (2012).
[51] C. Yuan, R. D. Fu, D. L. Sang, Y. Q. Yao, and X. Y. Zhang, The tensile properties and fracture behavior of gradient nano-grained/coarse-grained zirconium, Mater. Lett. **107**, 134 (2013).
[52] S. Cai, M. R. Daymond, R. A. Holt, M. A. Gharghouri, and E. C. Oliver, Evolution of interphase and intergranular stresses in Zr–2.5Nb during room temperature deformation, Mater. Sci. Eng. A **501**, 166 (2009).
[53] Z. N. Yang, F. C. Zhang, L. Qu, Z. G. Yan, Y. Y. Xiao, R. P. Liu, X. Y. Zhang, Formation of duplex microstructure in Zr–2.3Nb alloy and its plastic behaviour at various strain rates, Int. J. Plast. **54**, 163 (2014).
[54] V. Perovic, and G. C. Weatherly, The β to α transformation in a Zr-2.5 wt% Nb alloy, Acta Metall. **37,** 813 (1989).

[55] W. Z. Zhang, and G. R. Purdy, A TEM study of the crystallography and interphase boundary structure of α precipitates in a Zr-2.5 wt% Nb alloy, Acta Metall. Mater. **41,** 543 (1993).
[56] W. Z. Zhang, V. Perovic, A. Perovic, G. C. Weatherly, and G. R. Purdy, The structure of h.c.p.–b.c.c. interfaces in a Zr–Nb alloy, Acta Mater. **46,** 3443 (1998).

Figure 1

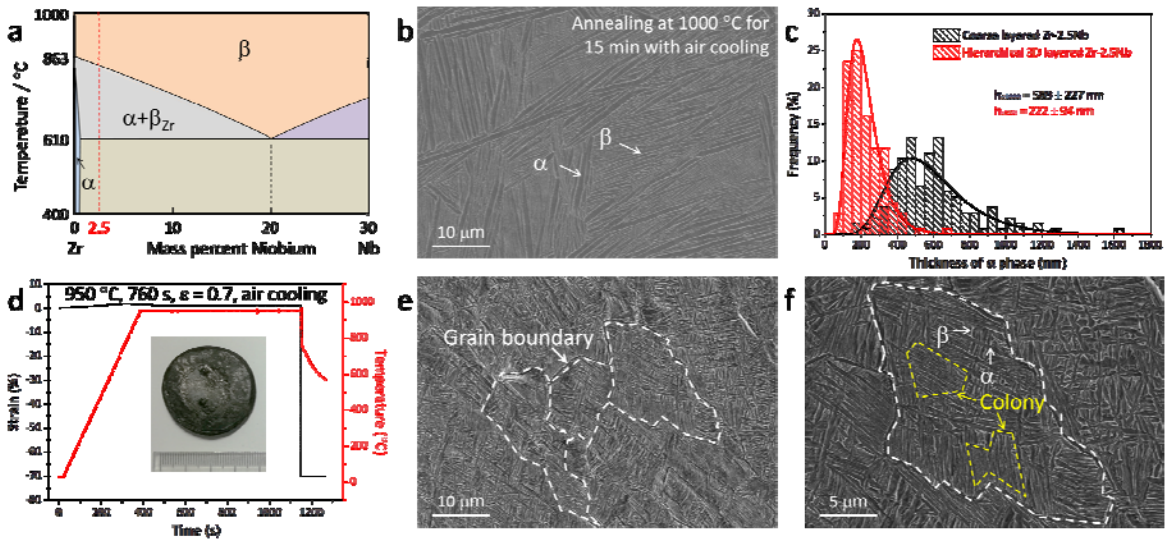

FIG. 1. (a) Zr-Nb binary phase diagram. (b) Microstructure of the coarse-layered (CL) Zr-2.5Nb. (c) Distribution of the phase thickness in the CL (the black one) and hierarchical 3D layered Zr-2.5Nb (the red one). (d) Temperature (the red one) and strain (the black one) vs time schedule associated with the DTMPT. (e) and (f) Hierarchical microstructure of 3D Zr-2.5Nb.

Figure 2

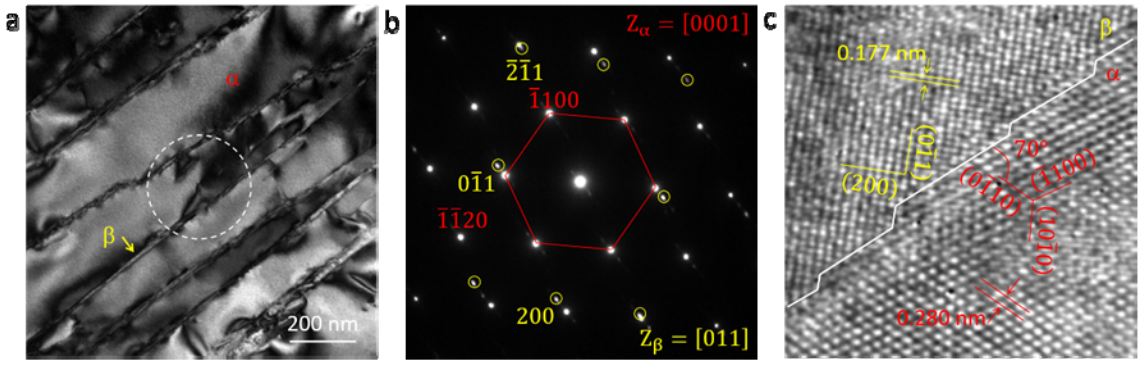

FIG. 2. (a) Duplex-phase in hierarchical 3D Zr-2.5Nb. (b) Two phases have a Burgers orientation relationship. (c) High-resolution TEM image of the α/β interface.

Figure 3

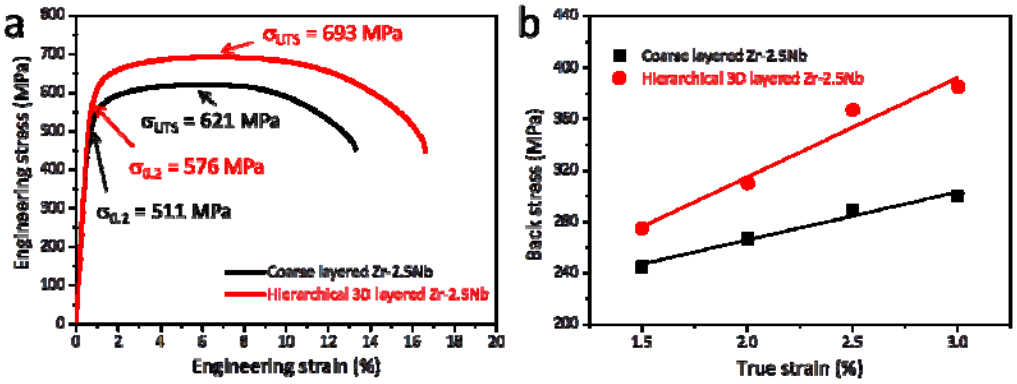

FIG. 3. (a) Engineering stress-strain curves for the CL and hierarchical 3D layered Zr-2.5Nb. (b) Variation of back stress with strain.

Figure 4

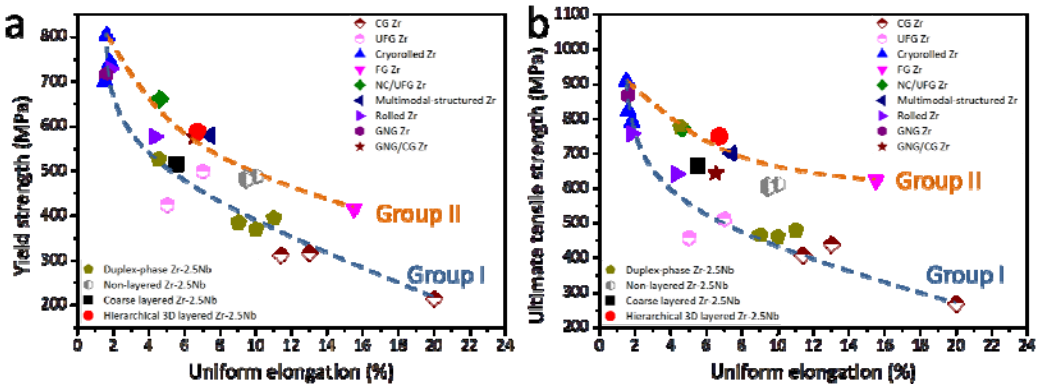

FIG. 4. (a) and (b) Comparison of the mechanical properties of hierarchical 3D layered Zr-2.5Nb with other Zr alloys[47-53]. Group I has homogeneous microstructures, and Group II has heterogeneous microstructures.

Figure 5

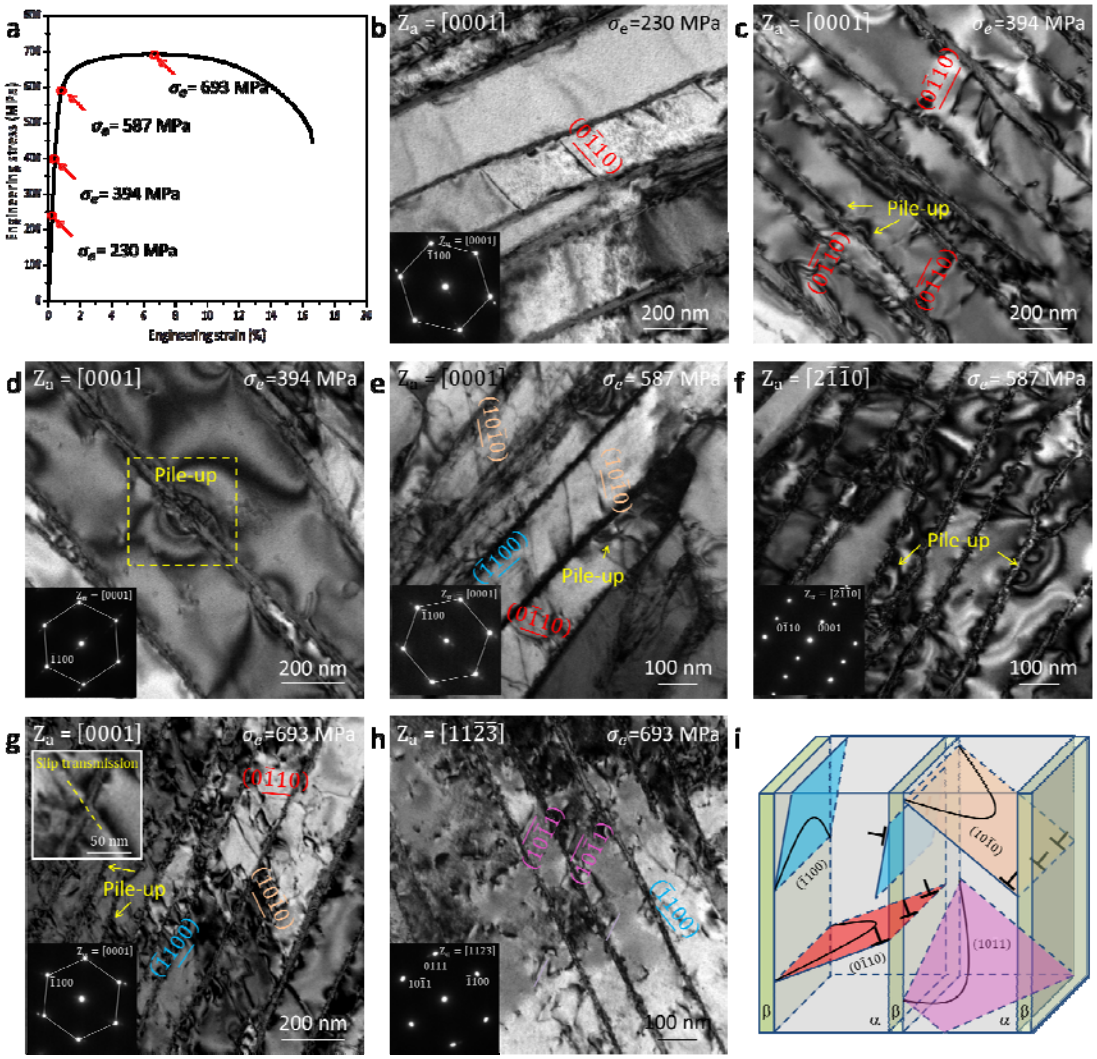

FIG. 5. Dislocation structures. (a) Tensile tests were interrupted at four critical stresses. (b) At σ_e=230 MPa. (c) and (d)At σ_e=394 MPa. (e) and (f) At σ_e=587 MPa. (g) and (h) At σ_e=693 MPa. (i) Illustration of the slip systems.